NASA Technical Paper 1772

Improved Method for Calculating Transonic Velocities on Blade-to-Blade Stream Surfaces of a Turbomachine

Jerry R. Wood

APRIL 1981

NASA

NASA Technical Paper 1772

Improved Method for Calculating Transonic Velocities on Blade-to-Blade Stream Surfaces of a Turbomachine

Jerry R. Wood
Lewis Research Center
Cleveland, Ohio

NASA
National Aeronautics
and Space Administration

Scientific and Technical
Information Branch

1981

Summary

A method has been developed which improves the accuracy of a NASA developed computer program used to calculate transonic velocities on a blade-to-blade surface of a turbomachine. Since the original program involves a solution to the stream-function equation on a stream surface using a finite-difference method, the flow must be totally subsonic. For this reason a reduced flow problem was defined whereby the finite-difference method was used to obtain a solution to the stream-function equation for a totally subsonic flow field. These streamlines for the reduced flow rate were then assumed to approximate those of the full mass flow rate. A solution at the full mass flow rate was then obtained by the velocity gradient method using the reduced flow streamlines. In some instances this velocity gradient method of solution is very sensitive around the leading and trailing edges of a turbomachine and may yield large velocity fluctutations. The method described in this report improves the accuracy of the assumption concerning the streamlines by preserving the stream-function equation in an approximate manner from the full mass flow to the reduced mass flow by suitably modifying the stream-sheet normal thickness (b). The method also provides an alternative way to obtain the transonic velocities, which eliminates the previously required velocity gradient method. Subsonic and slightly supersonic data from a two-dimensional compressor cascade and an axial turbine stator were compared with the numerical solutions. The results when using the modified method were in good agreement in both cases. The solution without the modified b compared well to the two-dimensional cascade results but differed significantly from the data for the turbine stator. It was also shown that instead of using the velocity gradient method with the modified b, a final transonic solution could be obtained by scaling the velocities obtained at the reduced mass flow rate by the reduction factor if the modified b was used. In all cases investigated the scaled solution was equal or superior to the solution obtained by the velocity gradient method. When using the present (modified stream-sheet thickness) method a much higher reduction factor is possible for a high pressure ratio centrifugal compressor impeller blade row than is possible with the original method.

Introduction

The NASA developed computer programs (refs. 1 to 3), used for obtaining blade-to-blade velocities in the blade rows of turbomachines, use the finite-difference technique for the solution of the stream-function equation. Difficulties arise when attempting to solve this equation with the finite-difference method when local supersonic velocities are present (see ref. 1); therefore, the entire flow field must be subsonic.

For transonic velocities the analysis program of reference 1, TSONIC, uses a technique where the stream-function equation is solved with the finite-difference method at a reduced mass flow rate. The reduced mass flow rate is chosen so that all velocities in the flow field are subsonic. The streamlines from this solution are assumed to closely approximate those of the full mass flow rate. The gradients and angles from these streamlines are used with the velocity gradient method (see ref. 1 for a discussion of this method) to obtain the transonic solution at the full mass flow rate. There are cases which involve large gradients in density and/or stream-sheet normal thickness where the method used in reference 1 does not adequately model the streamlines. Also, even in cases where the streamlines are well modeled, the velocity gradient method of solution is very sensitive around the entry and exit regions of a turbomachine blade row and may yield large velocity fluctuations. The method described in this report insures that the streamlines for the reduced flow solution are very close to those of the full mass flow solution by suitably preserving terms in the stream-function equation involving the density and stream-sheet normal thickness. The method also leads to an alternative technique for obtaining the final transonic solution that does not suffer from the problems encountered with the velocity gradient method in the entry and exit regions. The basic equations are derived and may be easily coded into the original programs of references 1 to 3. Several examples are presented to demonstrate the effect of the method when used on various blade rows. Two of the examples have experimental data at transonic velocities for comparison with the analytical solutions.

Symbols

A	$f(\beta, \alpha,$ streamline geometry)
a	area
b	stream-sheet normal thickness, m
C_p	specific heat at constant pressure, J/(kg)(K)
m	meridional streamline distance, m
N	number of blades
R_f	reduction factor
R	gas constant, J/(kg)(K)
r	radius from axis of rotation, m
S	length along blade surface, m
T	temperature, K
u	stream function
V	absolute fluid velocity, m/sec
W	fluid velocity relative to the blade, m/sec
w	mass flow per blade flowing through stream channel, kg/sec
α	angle between meridional streamline and axis of rotation, rad
β	angle between relative velocity and meridional plane, rad
γ	specific heat ratio
θ	relative angular coordinate, rad
λ	inlet angular momentum, $(rV_\theta)_{in}$
ρ	density, kg/m^3
ω	rotational speed, rad/sec

Subscripts:

av	average values across the channel
cr	critical velocity
in	inlet
LE	leading edge
m	component in direction of meridional streamline
r	conditions at reduced flow
TE	trailing edge
θ	tangential component

Superscripts:

$'$	absolute stagnation condition
$''$	relative stagnation condition

Analysis

General

The method in reference 1 assumes that the streamlines for the full and reduced flow cases will be approximately the same if the right hand side of equation (1) of reference 1 (repeated here) is

$$\frac{1}{r^2}\frac{\partial^2 u}{\partial \theta^2}+\frac{\partial^2 u}{\partial m^2}-\frac{1}{r^2}\frac{1}{\rho}\frac{\partial \rho}{\partial \theta}\frac{\partial u}{\partial \theta}+\left[\frac{\sin\alpha}{r}-\frac{1}{\rho b}\frac{\partial(\rho b)}{\partial m}\right]\times\frac{\partial u}{\partial m}=\frac{2b\rho\omega}{w}\sin\alpha \qquad (1)$$

maintained by preserving the ratio of rotational speed to mass flow rate, ω/w. The streamlines would be identical if the flow were incompressible since the coefficients on the left hand side involving gradients in density are zero, and the geometry terms are the same for the full flow-rate case and the reduced flow-rate case. However, for compressible flow, the coefficients will change if the mass flow rate is reduced. Reference 1 maintains ω/w by setting

$$\omega_r = \omega R_f \qquad (2)$$

$$w_r = w R_f \qquad (3)$$

where R_f is the reduction factor. The angular momentum, rV_θ, for the reduced flow rate at the leading and trailing edges is determined assuming that the relative flow angles input are the same for the reduced and full flow rates. The relative flow angles at the upstream and downstream boundaries of the flow field are calculated assuming conservation of angular momentum at the reduced flow rate between the blade edges and the boundaries. These boundary flow angles are used to determine the necessary boundary conditions for the stream-function solution. Since the relative flow angles and geometry at the leading and trailing edges are assumed to be the same for the reduced and full flow rates, $(\rho W)_r$ at the blade edges can be calculated from

$$(\rho W)_{r,av} = \frac{w_r}{a} = \frac{w_r N}{rb2\pi\cos\beta_{av}} \qquad (4)$$

This is equivalent to

$$(\rho W)_{r,av} = (\rho W)_{av} R_f \qquad (5)$$

However, equations (2) and (5) with relative flow angle preserved for the reduced mass flow case at the leading and trailing edges do not result in an absolute velocity diagram that is similar for the two mass flow

cases when the blade row is rotating. For the absolute and relative velocity triangles to be similar for the reduced and full mass flow cases, the relative velocity at the reduced mass flow rate must be

$$W_r = WR_f$$

if the rotation rate is reduced by the reduction factor (eq. (2)). This differs from equation (5) by the change in density from the full mass flow rate case to the reduced mass flow rate case. Since equation (5) does not yield similar absolute velocity triangles, an incorrect value of reduced flow angular momentum $(rV_\theta)_r$, will be calculated at the blade leading and trailing edges. Since angular momentum is conserved between the blade edges and the flow field boundaries, the relative flow angle at these boundaries will not be the same for the reduced flow and the full flow cases. The resultant streamlines obtained for the reduced flow case will have a different flow angle distribution and different curvatures from the boundaries to the blade edges than that for the full flow case. This effect on the flow angles at the boundaries is small except when large changes in radius occur such as at the exit of a centrifugal impeller blade row. This effect on reduced flow angular momentum will not occur when the blade row is stationary since the absolute flow angle is preserved.

In attempting to obtain a meaningful solution for the velocity gradient equation using the streamlines calculated at reduced flow rate, it is not sufficient to closely approximate the streamline geometry for the full flow rate (see ref. 1, p. 9). The velocity gradient equation is

$$\frac{\partial W}{\partial \theta} = AW + r \tan \beta \frac{\partial W}{\partial m} + \frac{2\omega r \sin \alpha}{\cos \beta} \tag{6}$$

where
$A = f(\beta, \alpha,$ streamline geometry)

Values for A and β are determined from the streamline geometry calculated at the reduced flow rate. The gradient in velocity, $\partial W/\partial m$, is obtained from

$$\frac{\partial W}{\partial m} = \frac{(\partial W/\partial m)_r}{R_f} \tag{7}$$

The remaining quantities r, ω, α are known inputs. In order to get a reasonable solution from the velocity gradient equation, $(\partial W/\partial m)_r/R_f$ must be reasonably close to that for the full flow rate. Since the streamlines for the reduced flow rate are used for the full flow case, then

$$\frac{\partial u}{\partial \theta} = \left(\frac{\partial u}{\partial \theta}\right)_r$$

and from reference 1

$$\frac{\partial u}{\partial \theta} = \frac{\rho b r W_m}{w} = \frac{\rho b r W \cos \beta}{w}$$

Now, the velocity at the reduced flow rate is related to that at the full flow rate by

$$(\rho W)_r = (\rho W) R_f$$

since

$$b_r = b,\ \beta_r = \beta \qquad \text{and} \qquad w_r = wR_f$$

from equation (3). Differentiation yields

$$\frac{\partial (\rho W)_r}{\partial m} = \frac{\partial (\rho W)}{\partial m} R_f$$

This differs from the assumed expression for $\partial W/\partial m$ (eq. (7)) in the velocity gradient equation (6) by the change in density between full and reduced flow rates. However, if the changes in density from the reduced flow rate to the full flow rate are not large, the effect on the solution by the velocity gradient method will probably be small (ref. (1)). When large changes in density occur, a better approximation for $\partial W/\partial m$ which accounts for compressibility is required. A method to account for the effects of compressibility is discussed next.

Modification for Solution of Streamfunction Equation at Reduced Flow Rate

The modification described here insures that the streamlines for the reduced flow case obtained from equation (1) will closely approximate those for the full flow case and that equation (7) will yield a good approximation of $\partial W/\partial m$ in equation (6) by accounting for the effect of compressibility. This is done by preserving the terms in equation (1) involving ρb in addition to those involving ω/w. That the stream-function equations would be preserved is evident if equation (1) is rewritten as

$$\frac{1}{r^2}\frac{\partial^2 u}{\partial \theta^2}+\frac{\partial^2 u}{\partial m^2}-\frac{1}{r^2}\frac{\partial u}{\partial \theta}\frac{\partial}{\partial \theta}(\ln \rho b)$$

$$+\left\{\frac{\sin \alpha}{r}-\frac{\partial}{\partial m}[\ln \rho b]\right\}\frac{\partial u}{\partial m}=2\rho b\frac{\omega}{w}\sin \alpha \qquad (8)$$

where b is assumed to be only a function of meridional distance, m. With the stipulation that ρb is preserved at each mesh point, equation (8) will yield the same stream-function solution for the reduced and full mass flow cases. From reference 1

$$\frac{\partial u}{\partial m}=-\frac{\rho b}{w}W_\theta \qquad (9)$$

$$\frac{\partial u}{\partial \theta}=\frac{\rho b r}{w}W_m \qquad (10)$$

Since $\partial u/\partial m$ and $\partial u/\partial \theta$ resulting from the solution of equation (8) are assumed to be the same for the reduced and full mass flow cases and since ρb is preserved, W_θ/w and W_m/w will be preserved. If the reduced mass flow rate is specified by equation (3), then

$$(W_\theta)_r=W_\theta R_f \qquad (11)$$

$$(W_m)_r=W_m R_f \qquad (12)$$

must also be true. Equations (2), (11), and (12) mean that not only is the relative velocity triangle—for a rotating blade row—for the reduced mass flow case similar to that for the full mass flow case at the leading and trailing edges, but the absolute velocity triangle is also similar since the tangent of the absolute flow angle is $(\omega r+W_\theta)/W_m$. This is a direct result of preserving ρb and ω/w in equations (1), (9), and (10). The streamlines so obtained from the reduced flow rate solution, which are to be used in the velocity gradient equation for the full flow rate, should closely approximate those of the full flow rate. Also, equations (11) and (12) yield

$$W_r=WR_f$$

so that

$$\frac{\partial W_r}{\partial m}=\frac{\partial W}{\partial m}R_f$$

and the second condition (see previous section) for a valid velocity gradient solution at full flow rate is satisfied.

Alternative to Velocity Gradient Method to Obtain Full Mass Flow Solution

There are cases where the velocity gradient solution in the entry and exit regions of a turbomachine blade row is extremely sensitive and may yield large velocity fluctuations. This sensitivity arises from the fact that second derivatives of the stream-function are required in the velocity gradient equation (appendix A of ref. 1). Small changes in calculated stream-function values as the flow passes the leading- and trailing-edge regions can result in large values of the second derivative. It would therefore, be advantageous to look for another way to obtain the final full mass flow solution. The present method, which preserves the stream-function equation by suitably modifying the stream-sheet normal thickness, b, provides for a different approach.

Equations (11) and (12) imply that a solution for the full mass flow can be obtained by simply scaling with the value of R_f the velocities obtained at the reduced mass flow even though some local velocities at the full mass flow exceed the local critical velocity. It is well known (refs. 4 and 7) that equation (8) is elliptic for subsonic flow and hyperbolic for supersonic flow. The terms that determine whether the equation is hyperbolic or elliptic arise from the derivatives of ρ.

Since equation (8) is nonlinear, the numerical solution done in references 1 and 2 is done in two levels of iterations (ref. 2). Equation (8), in the form of equation (1) is first linearized by specifying the density at each mesh point in the calculation grid. An inner iteration is used to solve the linearized equations. The nonlinear solution is approached by successively redefining the density at each mesh point using the results of the previous inner iteration. In this type of two-step procedure the linearized stream-function equation solved in the inner iteration is always elliptic. The outer iteration, where equations (9) and (10) are used to determine the velocity field and the next estimate on the field, is where the finite-difference method encounters difficulty since the value of the W term can be satisfied by either a subsonic or supersonic value of velocity. This value of velocity is used to update the density estimate at each mesh point for the next inner iteration. However, since the inner iteration solves a linearized equation that is always elliptic and the b terms are preserved, it should be possible to obtain a full-flow solution by applying equations (11) and (12) to the velocities obtained at the reduced flow. The efficacy

of this scaling technique is demonstrated by several numerical examples in a later section.

Approximate Method to Preserve ρb

Preservation of ρb throughout the passage for the reduced mass flow calculations implies a known solution to the full flow field. However, a suitable approximation can be made by preserving ρb on a one-dimensional basis across the channel. This can be done since some knowledge of a representative blade-to-blade flow velocity must be known in order to determine the proper stream-sheet normal thicknesses for input.

It remains to find an expression for ρb, so that equation (8) is approximately preserved for the reduced flow case. This can be done by suitably reducing the stream-sheet normal thickness from b to b_r. Thus,

$$\frac{b_r}{b} = \frac{\rho}{\rho_r} = \left[\frac{\rho/\rho''}{(\rho/\rho'')_r}\right]\frac{\rho''}{\rho_r''} \tag{13}$$

$$\frac{b_r}{b} = \left[\frac{1-(\gamma-1)/(\gamma+1)(W/W_{cr})^2}{1-(\gamma-1)/(\gamma+1)(W/W_{cr})_r^2}\right]^{1/(\gamma-1)}\frac{\rho''}{\rho_r''}$$

The ratio of relative total densities for the full and reduced flow cases is

$$\frac{\rho''}{\rho_r''} = \frac{\rho_{in}'(T''/T_{in}')^{1/(\gamma-1)}}{\rho_{in}'(T_r''/T_{in}')^{1/(\gamma-1)}} = \left(\frac{T''}{T_r''}\right)^{1/(\gamma-1)} \tag{14}$$

Also, since $W_{cr}^2 = \dfrac{2\gamma R}{\gamma+1}T''$ and $W_r = WR_f$

$$\left(\frac{W}{W_{cr}}\right)_r^2 = R_f^2\left(\frac{W}{W_{cr}}\right)^2\left(\frac{T''}{T_r''}\right) \tag{15}$$

Substituting (14) and (15) into (13) yields

$$\frac{b_r}{b} = \left(\frac{T''}{T_r''}\right)^{1/(\gamma-1)} \times \left[\frac{1-(\gamma-1)/(\gamma+1)(W/W_{cr})^2}{1-(\gamma-1)/(\gamma+1)R_f^2\,(T''/T_r'')(W/W_{cr})^2}\right]^{1/(\gamma-1)} \tag{16}$$

Since R_f and b are input to TSONIC it remains only to find T'', T_R'', and W/W_{cr}. The relative stagnation temperature, T'', is found from

$$T'' = T_{in}' - \frac{2\omega\lambda - (\omega r)^2}{2C_p} \tag{17}$$

where λ, the inlet angular momentum, is calculated as per reference 2, appendix B, for the full mass flow case. Because the relative velocity triangles and the absolute velocity triangles are similar on a one-dimensional basis for the reduced and full cases,

$$\lambda_r = \lambda R_f \tag{18}$$

and T_r'' is calculated from equation (17) using λ_r, ω_r, and T_{in}'. The only additional input is the relative critical velocity ratio, W/W_{cr}, which is consistent with the stream-sheet normal thickness distribution though the blade row for the full mass flow rate.

Method of Obtaining the Input Critical Velocity Ratio, W/W_{cr}

Stream-sheet normal thicknesses are usually obtained from axisymmetric solutions such as those of references 5 and 6. The input critical velocity ratios can also be obtained from these programs. The procedure used on the numerical examples in a later section was to input the critical velocity ratios from these programs and then check the value of the critical velocity ratio from the blade-to-blade analysis (TSONIC) at the 50 percent streamline obtained by scaling the reduced flow velocities by the reduction factor. This distribution of W/W_{cr} was compared with the original input values of W/W_{cr} and input for a new solution if they differed significantly. The initial distributions of W/W_{cr} obtained from the MERIDL program of reference 5 agreed very well with the distribution of W/W_{cr} obtained from TSONIC at the 50 percent streamline.

In some cases, such as the low solidity axial turbine stator in the numerical examples, the blade row does not provide a great deal of guidance to the flow and a MERIDL type of solution is not applicable. This is because the flow at midchannel does not follow the blade for a significant portion of the channel. For this case an initial guess on the W/W_{cr} distribution was obtained by assuming a linear variation between the leading and trailing edges. The distribution of W/W_{cr} at the 50 percent streamline was then used as input and iterated as above. The convergence for this case was quite rapid.

Numerical Examples

Five numerical examples are shown to assess the effect of the modification in stream-sheet normal thickness on the surface velocities for various blade rows. The first and second examples are a two-dimensional compressor cascade and a high solidity axial turbine stator, respectively, for which transonic data were available. The next two examples are a multiple-circular arc compressor stator and a low solidity axial turbine stator. The final example is the shroud line of a centrifugal compressor impeller for which vector diagrams at leading and trailing edges are shown as well as the surface velocities. Blade geometry is shown for all cases. Inputs to TSONIC (ref. 1) for all blade rows in the numerical examples are presented in the appendix.

NACA 65(12)-10 Cascade

The blade passage tested in reference 8 and shown in figure 1 consisted of NACA 65(12)-10 airfoils having a solidity of one with an inlet flow angle of 45° and an angle of attack of 16.5°. The blade row was tested over a range of inlet Mach numbers from 0.12 to 0.89 and employed end-wall suction to maintain a two-dimensional flow (i.e., stream-sheet normal thickness is constant through the blade row) up to an inlet Mach number of 0.61. As reported in reference 8, the suction system had insufficient capacity to remove the required amount of air at higher flows. Two cases were studied corresponding to inlet Mach numbers of 0.61 and 0.71. Although the 0.71 case was not strictly two-dimensional, only about a 2.6 percent contraction in stream-sheet normal thickness, b, occurred from the upstream measurement station to the downstream measurement station. The measured surface velocities for the quoted angle of attack and several numerical solutions are shown in figures 2(a) and (b). For the 0.61 case the solution in figure 2(a) is for a reduction factor of one obtained with the finite-difference solution to the stream-function equation and shows a peak surface velocity slightly higher than the peak experimental velocity. Pressure surface velocity is slightly low. The 0.71 case at a reduction factor of 0.9 is shown in figure 2(b). The velocities are scaled from the solution obtained by the finite-difference method at a reduced flow rate using the modified b. The peak suction-surface velocity is slightly higher than the peak experimental velocity whereas the pressure surface velocity is about 7 percent low over the first half of the chord. The solution obtained with the original method using the velocity gradient method and no modified b is very close to that obtained with the modified b.

To determine the sensitivity of the TSONIC solution

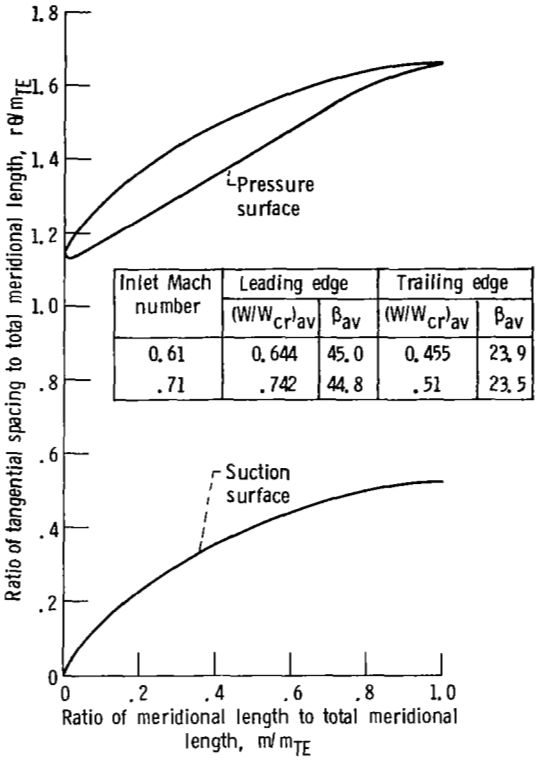

Inlet Mach number	Leading edge		Trailing edge	
	$(W/W_{cr})_{av}$	β_{av}	$(W/W_{cr})_{av}$	β_{av}
0.61	0.644	45.0	0.455	23.9
.71	.742	44.8	.51	23.5

Figure 1. - NACA 65(12)-10 compressor cascade blade section passage geometry, Total meridional length, m_{TE}, 0.067 meter.

to setting angle, the blade row was rotated 1° to an angle of attack of 15.5°. The agreement for the 0.61 Mach number case as shown in figure 3(a) is better than that previously shown for 16.5° angle of attack. The 0.71 Mach number case is shown in figure 3(b). Calculated surface velocities for both the modified b method and original method are close to the measured data.

Reference 9 also contains data for the 65(12)-10 blade row with the same solidity as in reference 8 but for a Mach number of about 0.09 and at various angles of attack. Comparison of the results of references 8 and 9 indicates that the angle of attack quoted in reference 8 may be too high by about 1°. Overall, the agreement between the numerical solutions and the experimental data is good at the angle of attack quoted in reference 8 and even better if an angle of attack of 15.5° is assumed.

The input critical velocity ratios required for the modified b method and the full flow rate b input for the 0.71 Mach number case are shown in figure 4. The modified b used for the reduced flow solution is also shown. The velocity and b change gradually through the blade row and thus the terms being affected by the present modified b method will be less significant than they would be for cases where large

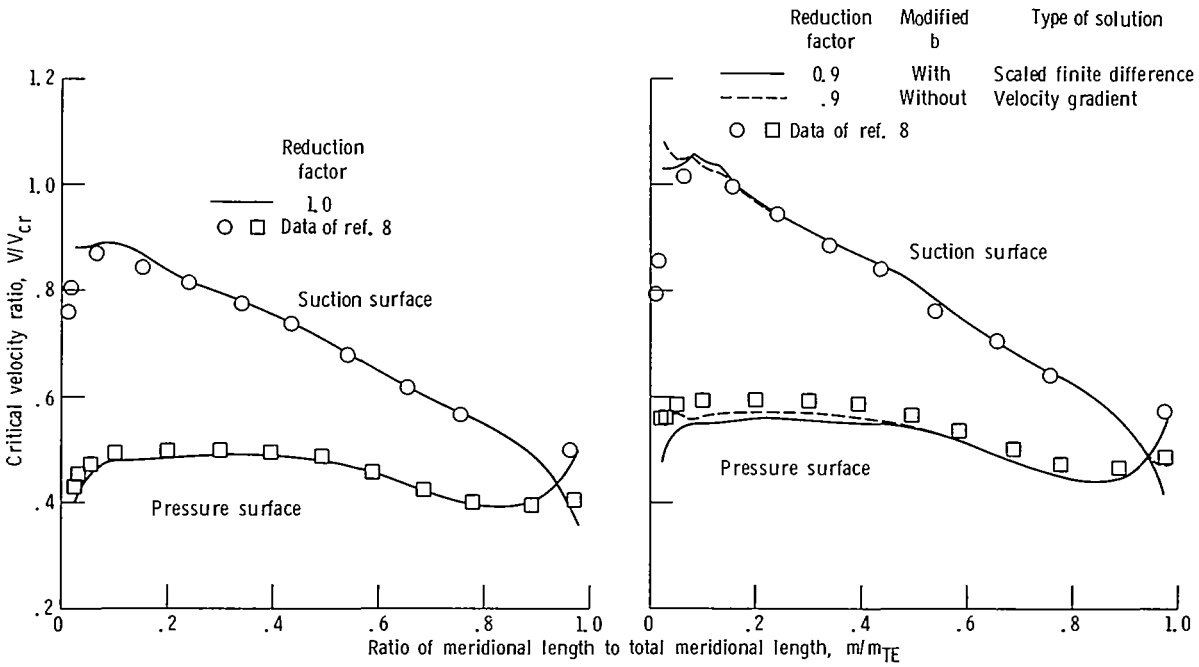

(a) Inlet Mach number, 0.61. (b) Inlet Mach number, 0.71.

Figure 2. - Calculated blade surface velocities on NACA 65(12)-10 compressor cascade blades and comparison with experimental data (ref. 8). Angle of attack, 16.5^0.

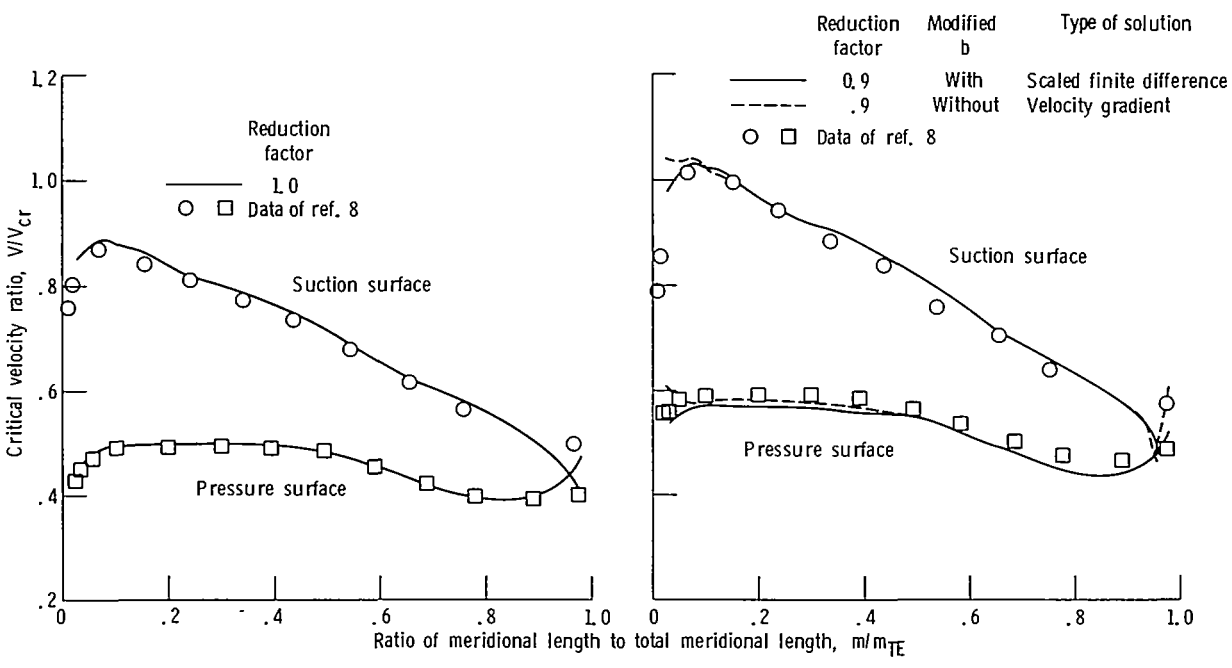

(a) Inlet Mach number of 0.61. (b) Inlet Mach number of 0.71.

Figure 3. - Calculated blade surface velocities on NACA 65(12)-10 compressor cascade blades at an angle of attack of 15.5^0 compared with data (ref. 8) at an angle of attack of 16.5^0.

gradients in b or velocity are present as will be shown later. The initial input critical velocity ratios were obtained from the MERIDL program of reference 5.

High Solidity Axial Turbine Stator

The mean section blade passage of the turbine stator tested in reference 10 is shown in figure 5. Data at design flow and at a slightly higher flow where transonic velocities are present are shown in figure 6. Figure 6(a) is the same case compared in reference 1, and has an inlet critical velocity ratio of 0.231. Figure 6(b) is for an inlet critical velocity ratio of 0.243 which corresponds to the hub critical velocity ratio of 1.1 from reference 10. In reference 1 the stream-sheet normal thickness was assumed to be constant through this stator. The present numerical solutions were obtained assuming a 3-percent contraction in stream-sheet normal thickness through the blade row. This is consistent with the estimated design total-pressure loss assumed in reference 10. According to reference 10, the design mass flow rate was achieved at the design static pressure ratio on both the inner and outer walls; this indicates that the 3 percent loss is reasonable. A comparison of the velocities obtained at a reduction factor of 0.8 with (1) the original velocity gradient method, (2) the scaled solution from the finite-difference method using the modified b, and (3) the velocity gradient method using the modified b is also shown in figure 6. The surface velocities shown in figure 6(a), calculated with the velocity gradient method both with and without the modified b agree well over most of the channel. However, over the latter 20 percent of the passage, the velocities obtained with both these solutions deviate considerably from the data. In contrast, the velocities obtained by scaling the reduced flow rate solution agree with the data on both surfaces.

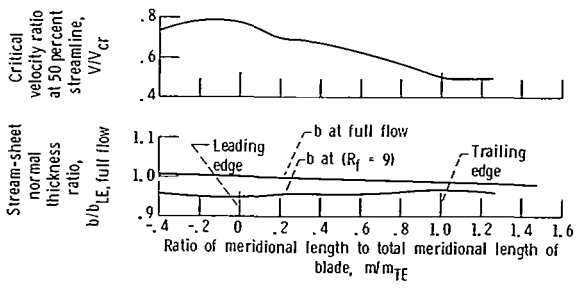

Figure 4. - Meridional distribution of critical velocity ratio at the 50 percent streamline and of the stream-sheet normal thickness for NACA 65(12)-10 compressor cascade blades. Inlet Mach number, 0.71.

Hub critical velocity ratio	Leading edge		Trailing edge	
	$(W/W_{cr})_{av}$	β_{av}	$(W/W_{cr})_{av}$	β_{av}
0.896	.231	0	0.778	-67.0
1.1	.243	0	.90	-67.0

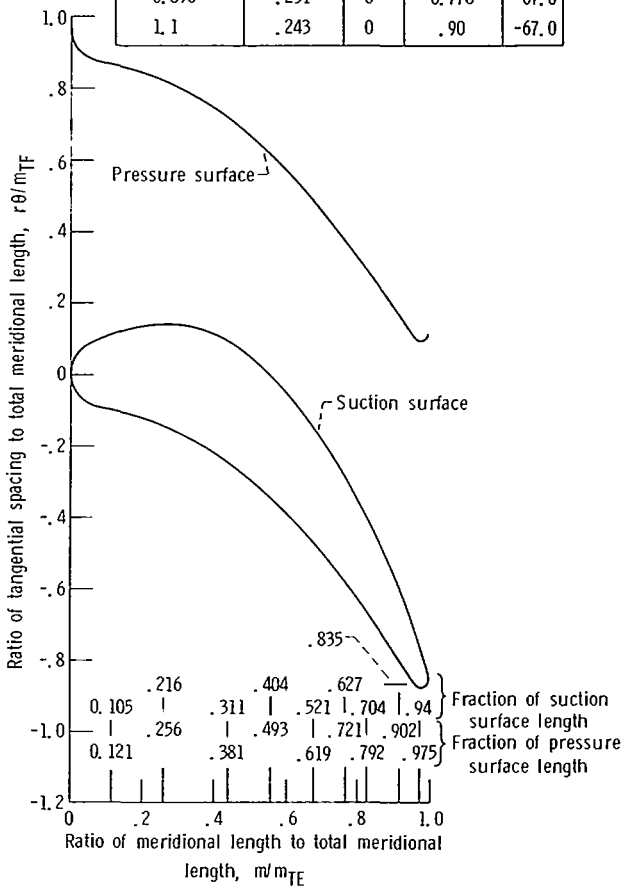

Figure 5. - High solidity turbine stator blade section passage geometry. Total meridional length, m_{TE}, 0.0429 m.

In figure 6(b) the surface velocities obtained from the velocity gradient method without the modified b deviate significantly from the data over much of the suction surface. The velocities obtained with the velocity gradient method and with the modified b, agree over most of the channel but deviate significantly from the data over the last 20 percent of the channel. As before, for the lower value of inlet critical velocity ratio, the velocities obtained by scaling the reduced flow solution agree well with the data on both surfaces.

The input critical velocity ratios required in the modified b method, the full flow rate b for the different inlet critical velocity ratios, and the resulting modified b values at the reduced flow rate are shown in figure 7. The gradients in b and velocity through the blade row are significantly greater than those in the previous example (see fig. 4). The input critical velocity ratios were initially obtained from

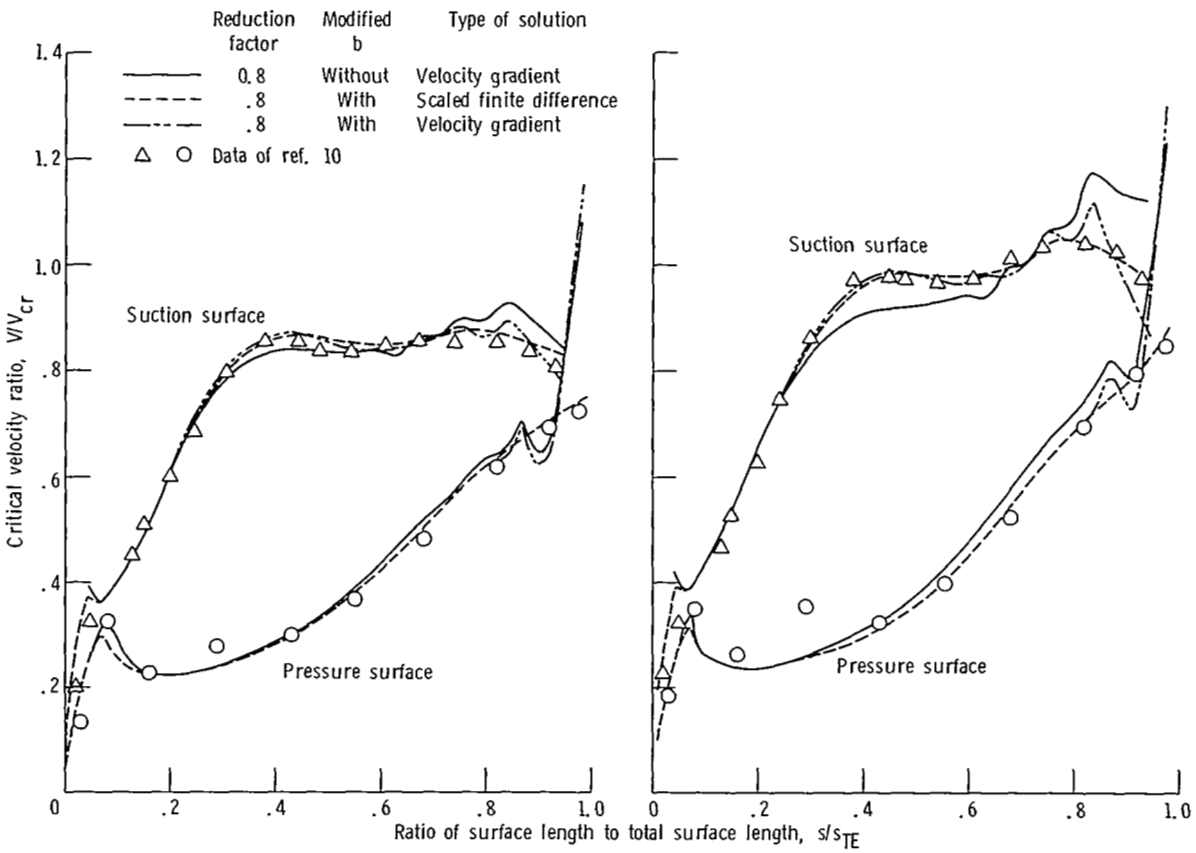

Figure 6. - Calculated blade surface velocities on high solidity turbine stator blade row and comparison with experimental data (ref. 10).

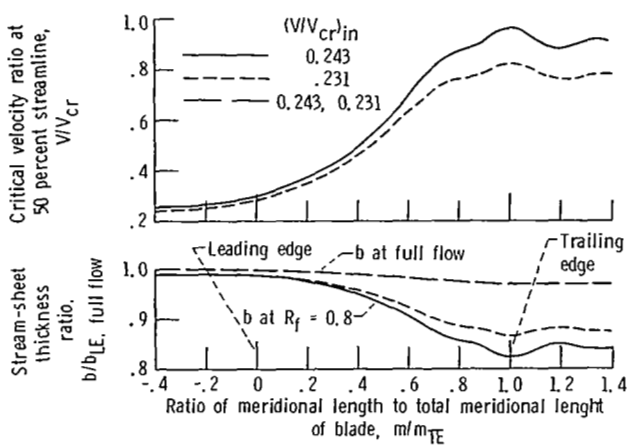

Figure 7. - Meridional distribution of critical velocity ratio at the 50 percent streamline and of the stream-sheet normal thickness for the high solidity turbine blade at inlet critical velocity ratios of 0.231 and 0.243.

calculated velocity diagrams at the leading and trailing edges.

Multiple Circular Arc Compressor Stator

The flow passage is shown in figure 8. Surface velocities obtained with the finite-difference method at a reduction factor of 1.0 (baseline solution) and velocities obtained from the velocity gradient method with a reduction factor of 0.8 and no modification to the *b* are shown in figure 9(a). The agreement is generally good except in the midchord region where the baseline solution shows a slightly higher peak velocity. The velocities obtained from (1) the baseline solution, (2) the velocity gradient method using the modified *b* at a reduction factor of 0.8, and (3) scaling the reduced-flow velocities when using the modified *b* at a reduction factor of 0.8 are compared in figure 9(b). Both solutions agree with the baseline solution.

The input critical velocity ratios for the modified *b* method and the *b* used at full flow rate and calculated for use at the reduced flow rate are shown

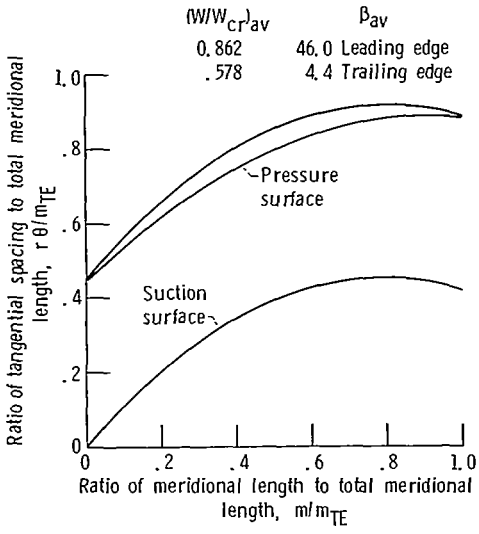

Figure 8. - Multiple-circular-arc compressor stator blade section passage geometry. Total meridional length, m_{TE}, 0.03444 meter.

in figure 10. The largest slopes in velocity ratio and b occur in the 30 to 40 percent region where the solution without the modification in *b* differed most from the baseline solution. The gradients in *b* and critical velocity ratio are much larger in this case than they were for the cascade of example A (see fig. 4). The input critical velocity ratios were initially obtained from the MERIDL program of reference 5.

Low Solidity Axial Turbine Stator

The stator blade-to-blade flow path is shown in figure 11. Comparisons of the baseline solution obtained with the finite-difference method at a reduction factor of 1.0 to the solution from the velocity gradient method using a reduction factor of 0.8 without a modification to the *b* and the solution from the velocity gradient method using a reduction factor of 1.0 are made in figure 12(a). The solution by the velocity gradient method of 0.8 without the modified *b* differs significantly from the baseline solution over both surfaces. The solution by the velocity gradient method at a reduction factor of 1.0 differs from the baseline solution in the leading edge region on the suction surface and near the trailing edge on the pressure surface. Figure 12(b) shows the baseline solution, the scaled solution from the finite-difference method at a reduction factor of 0.8 using the modified *b*, and the solution from the velocity gradient method at a reduction factor of 0.8 using the modified *b*. The solution from the velocity gradient method differs from the baseline solution on the suction surface near the leading edge and near the trailing edge on the pressure surface. As in the second example, the velocity ratios obtained by scaling the velocities from the finite-difference method at the reduced flow rate at a reduction factor of 0.8 are close to the baseline solution over both blade surfaces.

The *b* at full flow rate and the critical velocity ratios input for the modified b solution are shown in figure 13. The change in critical velocity ratio through the blade row is much greater than in the first and third examples (see fig. 4 and 10). The critical velocity ratios were initially obtained from the calculated velocity diagrams at the leading and trailing edges.

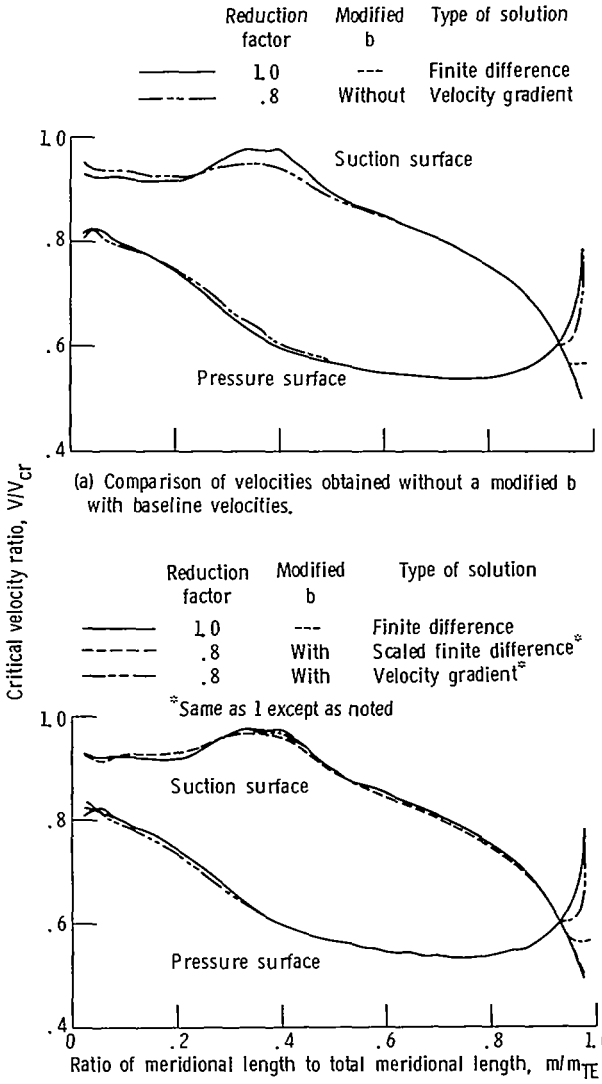

Figure 9. - Comparisons of calculated blade surface velocities obtained by finite difference (baseline velocities) scaled finite difference, and velocity gradient methods. Multiple circular-arc-compressor stator blades; inlet critical velocity ratio, 0.862.

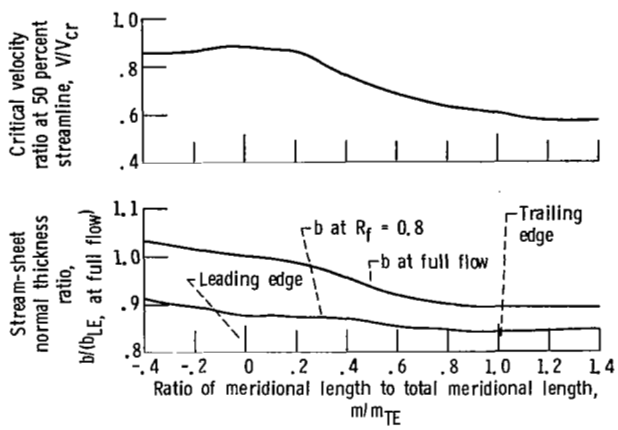

Figure 10. - Meridional distribution of critical velocity ratio at 50 percent streamline and of the stream-sheet normal thickness for multiple-circular-arc compressor stator. Inlet critical velocity ratio, 0.862.

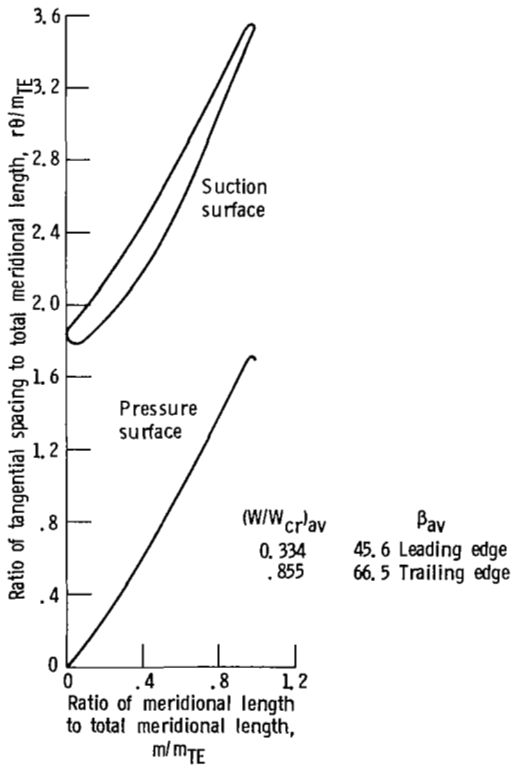

Figure 11. - Low solidity turbine stator blade section passage geometry. Total meridional length, m/m_{TE}, 0.0127 meter.

Centrifugal Compressor Impeller Shroud Line

The tangential spacing versus meridional distance of a centrifugal compressor impeller shroud line designed for a total pressure ratio of about 9:1 is shown in figure 14. The design free-stream velocity diagrams for this impeller are shown in figure 17 and will be discussed later. Since the flow entering the blade row is supersonic, it is likely that some shocks will be present in the entry region. The program of reference 1 assumes shock-free flow or, at worst, very weak shocks in the flow. A modification was made to the program of reference 1 to allow shock-free entry to be calculated with the velocity gradient method when the mean flow is slightly supersonic. The procedure is similar to that used in reference 5. No shocks should exist in the impeller past the 10 to 15 percent chord location since a normal shock at the blade leading edge would probably hit the suction surface in this region (see fig. 14).

Based on the results obtained with the previous examples, it is concluded that the solution obtained with the velocity gradient method with the modified b will yield a better solution in the passage than the solution from the velocity gradient method without the modified b when the critical velocity ratio and b vary significantly through the channel as they do in this example. A comparison of the solutions obtained with a modified b at a reduction factor of 0.8 and without a modified b at a reduction factor of 0.2 is made in figure 15. These values were the highest reduction factors that could be used with the respective methods. The reason such a low reduction factor was required for the case without the modified b will be discussed later. The solution obtained with the velocity gradient method and without the modified b differs significantly from that obtained with the velocity gradient method and the modified b. The difference occurs primarily from the fact that the gradient in velocity $\partial W_r/\partial m$ obtained from the reduced flow solution and used in the velocity gradient equation (see Analysis—General) does not yield a good approximation to the gradient in velocity at the full flow rate. The reason for this will be discussed shortly. The solution obtained by scaling the velocities calculated at the reduced flow rate at a reduction factor of 0.8 agrees well with the solution from the velocity gradient method for the modified b case.

The stream-sheet normal thickness and critical velocity ratio input for the modified b case are shown in figure 16. The critical velocity ratio distribution was initially obtained from the axisymmetric program of reference 6. The modified b at the reduced flow rate is clearly larger than the b at full flow rate over most of the channel and demonstrates why the modified b method permits a higher reduction factor to be used than could be used with the original method where the b at the reduced flow rate was the same as for the full flow rate. The b at the trailing edge for the reduced flow rate is nearly 50 percent larger than the b at the trailing edge for the full flow-rate.

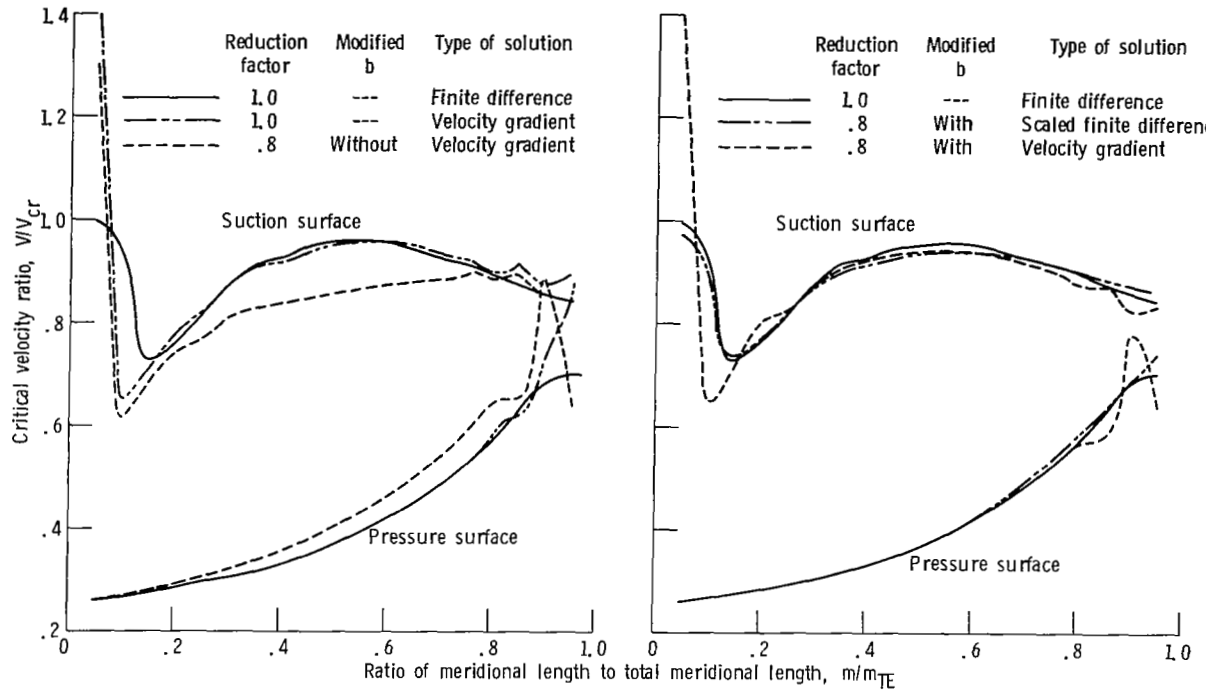

(a) Comparison of velocites obtained from the velocity gradient method at two reduction factors and without modified b to the baseline velocities.

(b) Comparison of velocities obtained with a modified b to baseline velocities.

Figure 12. - Comparison of calculated blade surface velocities obtained by finite difference (baseline velocities) scaled finite difference, and velocity gradient methods. Low solidity turbine stator blades; Inlet critical velocity ratio, 0.334.

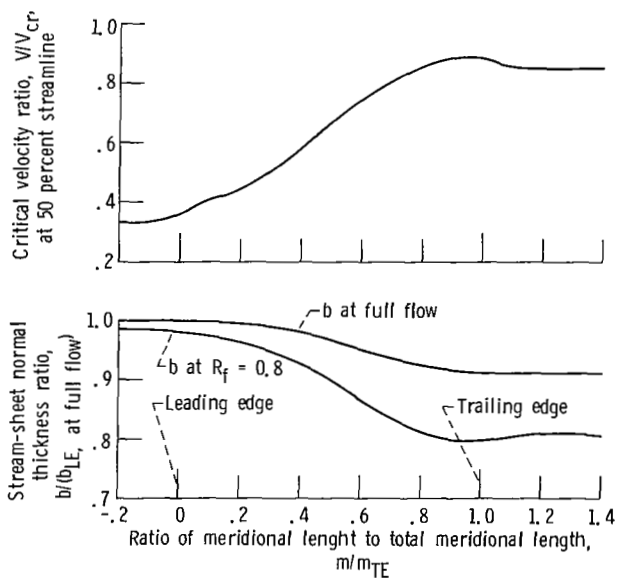

Figure 13. - Meridional distribution of critical velocity ratio at 50 percent streamline and of stream-sheet normal thickness for low solidity turbine stator blades. Inlet critical velocity ratio, 0.334.

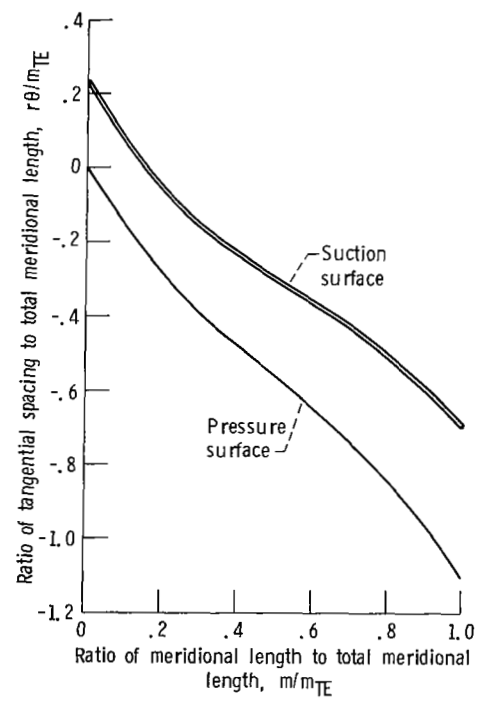

Figure 14. - Centrifugal compressor impeller shroud line section passage geometry. Total meridional length, m_{TE}, 0.0632 meter.

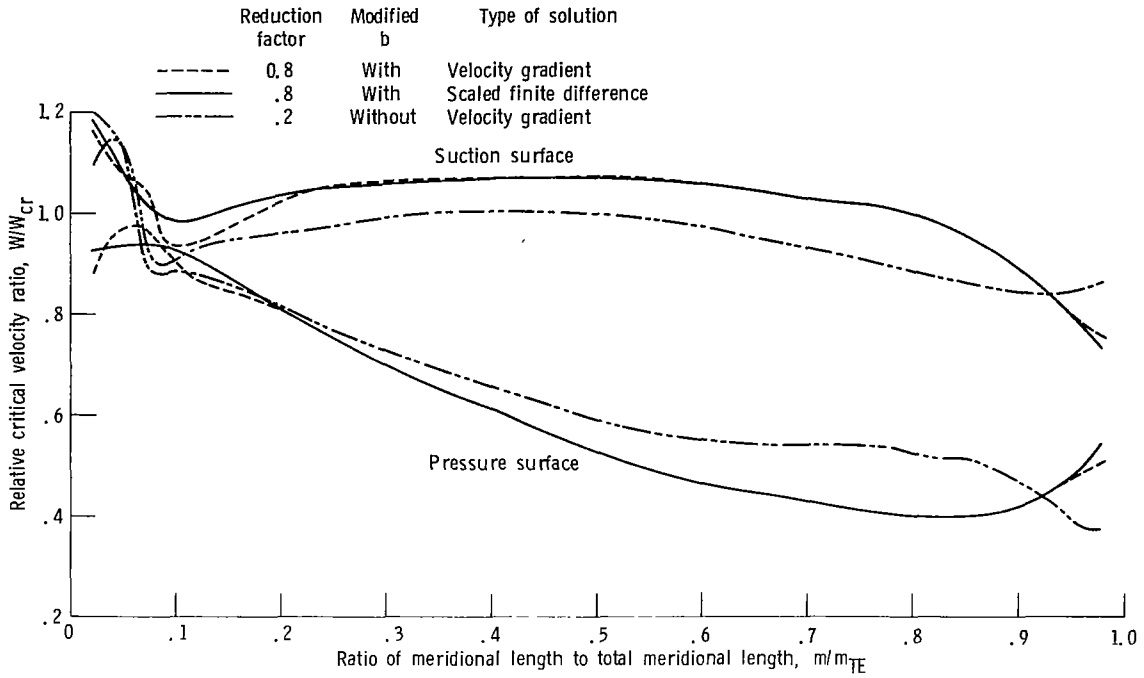

Figure 15. - Calculated blade surface velocities for centrifugal compressor impeller shroud line. Inlet relative critical ratio, 1.168.

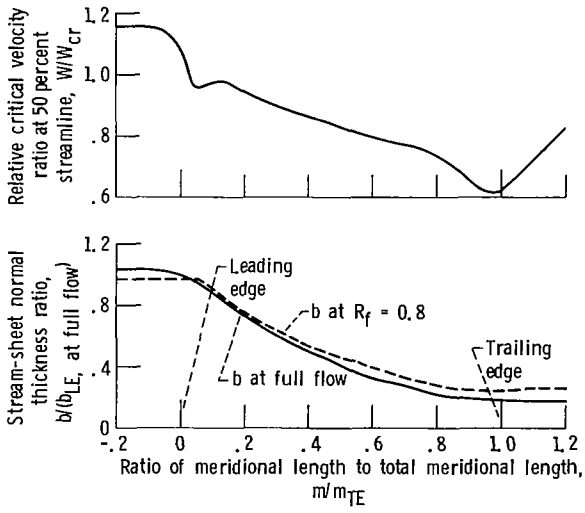

Figure 16. - Meridional distribution of relative critical velocity ratio at the 50 percent streamline and of the stream-sheet normal thickness for the centrifugal compressor impeller shroud line. Inlet relative critical velocity ratio, 1.168.

A comparison of the velocity diagrams at the leading and trailing edges for the centrifugal impeller for the full mass flow rate, the reduced mass flow rate without the modified b at a reduction factor of 0.2, and the reduced mass flow rate with the modified b at a reduction factor of 0.8 is made in figure 17. The full flow diagrams have an inlet absolute flow angle of 0° and an outlet absolute flow angle of 68.8°. The case without the modified b at a reduced flow rate has an inlet absolute flow angle of 17.7° and an outlet absolute flow angle of 8.05°. The relative flow angles are specified in the analysis to be the same for both full and reduced flows. Both the absolute and relative velocity diagrams for the reduced flow case with the modified b are similar to those for the full flow rate. These average quantities at the blade edges in figure 17 can be used to approximate $\partial W/\partial m$ to demonstrate why the velocity gradient solution without the modified b differs significantly from that obtained with the modified b. As shown by the equation in figure 17, $\partial W/\partial m$ obtained without the modified b is -6703 meters per second per meter compared with 2458 meters per second per meter for the full flow rate, and 2445 meters per second per meter for the case with the modified b.

The effect of reduction factor on some one-dimensional flow parameters at impeller inlet and exit when the stream-sheet normal thickness b is not modified is shown in figure 18. It illustrates why a reduction factor as low as 0.2 was required for a fully subsonic flow. At the inlet (fig. 18(a)) the relative critical velocity ratio decreases almost linearly with reduction factor from 1.168 at a reduction factor of 1.0 to 1.0 at a reduction factor of 0.88. As the inlet

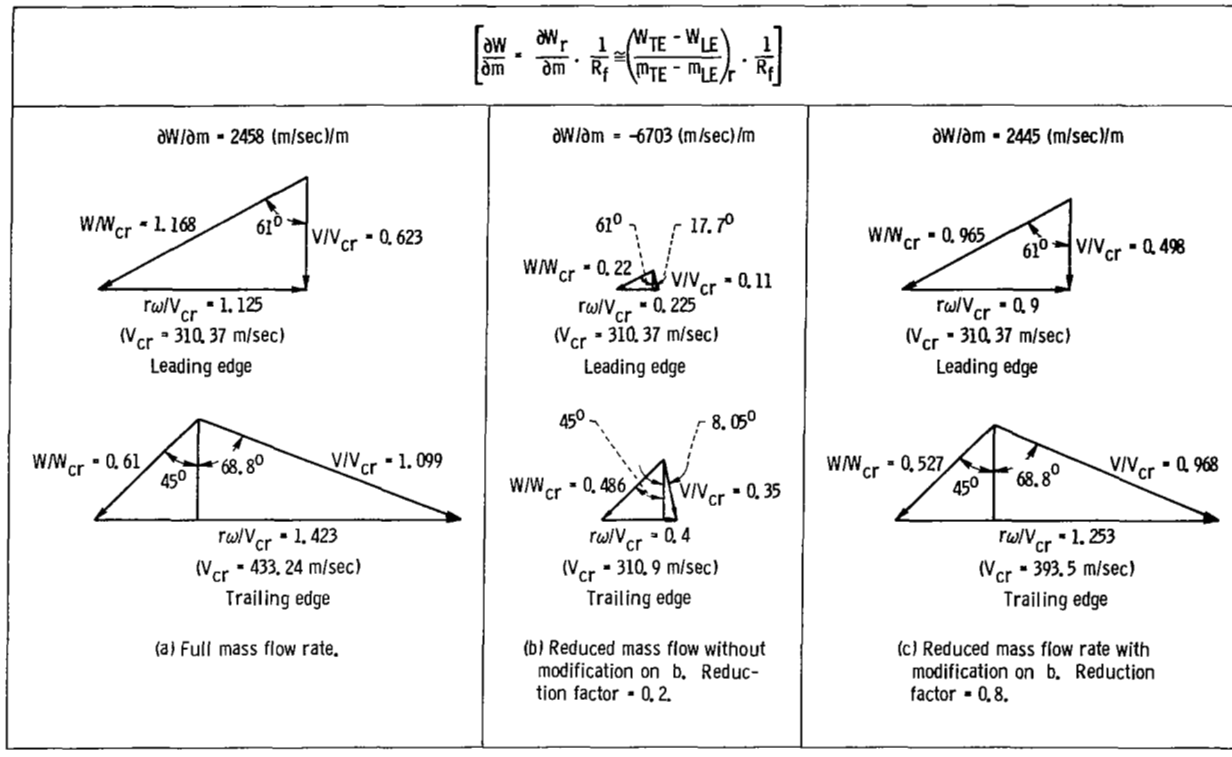

Figure 17. - Comparison of velocity diagrams at blade edges for the centrifugal compressor impeller shroud line for cases with and without a modification to the stream-sheet normal thickness to the velocity diagrams for the full mass flow rate. The reduction factors used represent the maximum values possible without supersonic velocities occuring in the blade row.

velocity ratio decreases to a point where all surface velocities in the inlet region would be subsonic (approximately a reduction factor of 0.85) the exit velocity ratio rises rapidly to a value of one. Between a reduction factor of 0.85 and 0.33, the exit is choked for the conditions used in the reduced flow calculations. Velocities on the blade surfaces are higher than the one-dimensional velocities, and a value of reduction factor of 0.2 was necessary in order for all velocities to be subsonic. The reason the exit velocity increases as reduction factor is reduced can be seen from manipulation of equation (4) where the flow quantities are average values:

$$(\rho W)_r = \frac{w_r N}{2\pi r b \cos\beta} \tag{4a}$$

$$\left(\frac{\rho W}{\rho'' W_{cr}}\right)_r = \frac{w R_f N}{\rho_r'' W_{cr,r} 2\pi r b \cos\beta} \tag{19}$$

using

$$\rho_r'' = \left(T_r''/T_{in}'\right)^{1/(\gamma-1)} \rho_{in}'$$

$$\left(T_r''/T_{in}'\right) = 1 + \frac{(r\omega_r)^2}{2C_p T_{in}'}$$

$$= 1 + \frac{\gamma-1}{\gamma+1}\left(\frac{r\omega R_f}{V_{cr,in}}\right)^2$$

(this is eq. (17) assuming $\gamma = 0$ at full and reduced flow rates) and

$$W_{cr,r} = \left(\frac{2\gamma}{\gamma+1} R T_r''\right)^{1/2}$$

equation (19) becomes

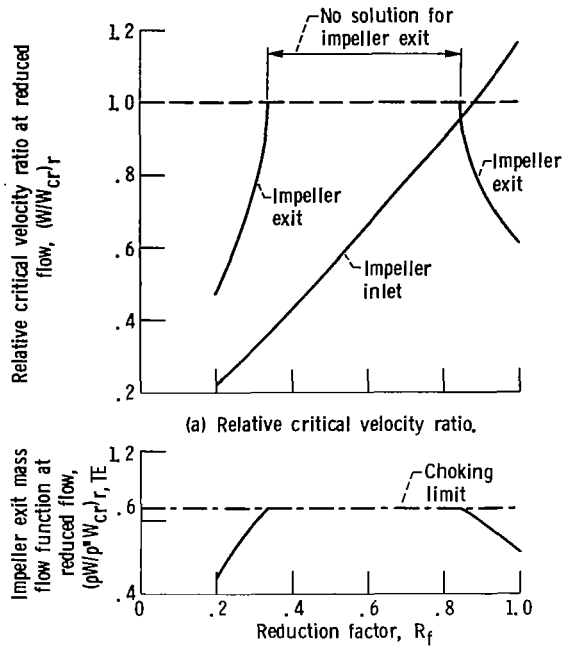

Figure 18. - Effect of reduction factor on conditions at leading and trailing edges of centrifugal compressor impeller shroud line assuming no modification in stream-sheet normal thickness.

$$\left(\frac{\rho W}{\rho'' W_{cr}}\right)_r$$

$$= \frac{wR_f N}{\rho'_{in}\left(\frac{T''_r}{T'_{in}}\right)^{1/(\gamma-1)}\left(\frac{2\gamma R}{\gamma+1}T''_r\right)^{1/2} 2\pi rb\cos\beta\left(\frac{T'_{in}}{T'_{in}}\right)^{1/2}}$$

$$= \frac{wR_f N}{\left(\frac{T''_r}{T'_{in}}\right)^{(1+\gamma)/2(\gamma-1)} \rho'_{in} V_{cr,in} 2\pi rb\cos\beta}$$

$$= \frac{wR_f N}{\rho'_{in} V_{cr,in} 2\pi rb\cos\beta\left[1+\frac{\gamma-1}{\gamma+1}R_f^2\left(\frac{r\omega}{V_{cr,in}}\right)^2\right]^{(1+\gamma)/2(\gamma-1)}}$$

For the centrifugal compressor impeller this becomes, for $\gamma = 1.4$,

$$\left(\frac{\rho W}{\rho'' W_{cr}}\right)_r = \frac{2.36157R_f}{(1+0.65756R_f^2)^3} \tag{20}$$

The maximum value of $(\rho W/\rho'' W_{cr})$ at a W/W_{cr} of 1 is 0.6339 for $\gamma = 1.4$. A value of $\rho W/\rho'' W_{cr}$ from equation (20) exceeding this maximum value as shown in figure 18(b) indicates that the required mass flow is too large for the assumed conditions (i.e., $\beta = \beta_r$, $\omega_r = \omega R_f$, $w_r = wR_f$, $b = b_r$) at the reduced flow rate.

Concluding Remarks

The modified b (stream-sheet normal thickness) method described herein significantly improves the capability of the computer program of reference 1 in cases where large gradients in velocity and/or stream-sheet normal thickness occur through the blade row. The method is relatively insensitive to the value of reduction factor used. For the low solidity turbine stator, solutions obtained by scaling the velocities from the reduced flow solution were very close for reduction factors of 0.6, 0.8, and 1.0. Similar results were obtained for the centrifugal compressor impeller using reduction factors of 0.1, 0.6, and 0.8. The fact that the transonic solution can be obtained by scaling the velocities obtained at the reduced flow rate effectively eliminates the need for the velocity gradient solution. Based on the data presented and on comparisons with other transonic methods (see, for example, the numerical method used in ref. 11), the solutions obtained with TSONIC appear to be valid up to a surface Mach number of about 1.1. For the type of shockless compressor cascade blading described in reference 11, TSONIC underpredicts the surface velocities in regions where the surface Mach numbers exceed 1.1 but accurately predicts the velocities over the rest of the blade.

Summary of Results

A method has been developed which improves the accuracy of an existing computer program used to calculate the blade-to-blade transonic velocities in a flow channel of a turbomachine. The method can be easily incorporated into published computer programs and requires only one additional input. The following were demonstrated in the numerical examples:

(1) Blade surface velocities obtained for a two-dimensional compressor-cascade agreed closely with subsonic data. Blade surface velocities at slightly transonic velocities agreed well on the suction surface but were slightly low on the pressure surface. The present method and the original method did not differ significantly beyond the leading edge for this example.

(2) Blade surface velocities obtained for a turbine stator compared well for subsonic and slightly transonic experimental velocities when using the present method. The numerical solutions obtained with the original method differed appreciably from the experimental data. This results from the larger gradients in velocity through the turbine blades compared with that of the compressor blades.

(3) In all cases investigated the transonic solution obtained by scaling the velocities calculated at the reduced flow rate by the reduction factor was equal or superior to the solution obtained with the velocity gradient equation when using the present method.

(4) When using the present method a much higher reduction factor is possible for a high pressure ratio centrifugal compressor impeller blade row than is possible with the original method.

Lewis Research Center
National Aeronautics and Space Administration
Cleveland, Ohio, October 3, 1980

Appendix—Input for Numerical Examples

The computer symbols used in this program are the same as those defined and used in reference 1 with the following exceptions:

(1) FSMI, FMSO: These allow input conditions at other than the leading and trailing edges. The option was used to input flow angles (for the second example) at an inlet Mach number of 0.71 at the measurement stations used in reference 8.

(2) SSM1, SSM2: These designate the meridional coordinates between which a supersonic mean flow is calculated by the velocity gradient method in the example for a centrifugal compression impeller shroud line.

(3) WOWCR: The critical velocity ratio input for each value of stream-sheet thickness at full mass flow rate.

(4) PLOSS: An array of fractional loss in total pressure which was used to modify the stream-sheet thickness internally in the fourth example.

NACA 65(12)-10 CASCADE AT 0.61 INLET MACH NUMBER AND 15.5 DEGREE ANGLE OF ATTACK

GAM	AR	TIP	RHOIP	WTFL		OMEGA	ORF
1.400000	1716.480	519.9993	0.2371500E-02	0.2304700E-02	0.0000000	0.0000000	1.912700
BETAI	BETAO	CHORDF	STGRF	FSMI	FSMO		
45.08749	23.91283	0.2186100	0.1208600E-03	0.0000000	0.0000000		
REDFAC	DENTOL	SSM1	SSM2				
0.9999999	0.9999999E-03	0.0000000	0.0000000				

MBI	MBO		MM	NBBI	NBL	NRSP
18	58	0 0	68	35	25145	28

BLADE SURFACE 1 -- UPPER SURFACE

RI1	RO1	BETI1	BETO1	SPLNO1			
0.6549999E-02	0.3614998E-03	69.00000	6.000000	9.000000			
MSP1 ARRAY							
0.0000000	0.5912997E-02	0.2121500E-01	0.4517600E-01	0.7546794E-01	0.1091400	0.1429110	0.1734100
0.0000000							
THSP1 ARRAY							
0.0000000	0.1262000E-04	0.3091000E-04	0.5209999E-04	0.7315999E-04	0.9089000E-04	0.1037500E-03	0.1128900E-03
0.0000000							

BLADE SURFACE 2 -- LOWER SURFACE

RI2	RO2	BETI2	BETO2	SPLNO2			
0.2075000E-02	0.3614998E-03	20.00000	11.00000	9.000000			
MSP2 ARRAY							
0.0000000	0.6136999E-02	0.2158700E-01	0.4565000E-01	0.7597995E-01	0.1095999	0.1432199	0.1735600
0.0000000							
THSP2 ARRAY							
0.0000000	-0.2199999E-06	0.9590000E-05	0.2498699E-04	0.4383999E-04	0.6455000E-04	0.8609999E-04	0.1039600E-03
0.0000000							

MR ARRAY

-0.1507559	-0.1040879	-0.1099000E-01	-0.5500000E-02	0.1099000E-01	0.1649700E-01	0.3299000E-01	0.4820100E-01
0.6293797E-01	0.7767498E-01	0.9241396E-01	0.1071530	0.1218910	0.1366280	0.1513669	0.1661060
0.1808430	0.1955810	0.2103200	0.2250650	0.2398199	0.2545649	0.2693040	0.2953039
0.3213020	0.3473020	0.3733020	0.3993030				

RMSP ARRAY

1000.500	1000.500	1000.500	1000.500	1000.500	1000.500	1000.500	1000.500
1000.500	1000.500	1000.500	1000.500	1000.500	1000.500	1000.500	1000.500
1000.500	1000.500	1000.500	1000.500	1000.500	1000.500	1000.500	1000.500
1000.500	1000.500	1000.500	1000.500				

BESP ARRAY

0.9999998E-02	0.9999998E-02	0.9999998E-02	0.9999998E-02	0.9999998E-02	0.9999998E-02	0.9999998E-02	0.9999998E-02
0.9999998E-02	0.9999998E-02	0.9999998E-02	0.9999998E-02	0.9999998E-02	0.9999998E-02	0.9999998E-02	0.9999998E-02
0.9999998E-02	0.9999998E-02	0.9999998E-02	0.9999998E-02	0.9999998E-02	0.9999998E-02	0.9999998E-02	0.9999998E-02
0.9999998E-02	0.9999998E-02	0.9999998E-02	0.9999998E-02				

WOWCR ARRAY

0.6461000	0.6443300	0.6820000	0.6790000	0.6640000	0.6569999	0.6339999	0.6215700
0.6156700	0.6044500	0.5966600	0.5868100	0.5747100	0.5607800	0.5446200	0.5304500
0.5158899	0.5040300	0.4811500	0.4549699	0.4553500	0.4535600	0.4551100	0.4552700
0.4546400	0.4550800	0.4549000	0.4556600				

PLOSS ARRAY

0.0000000	0.0000000	0.0000000	0.0000000	0.0000000	0.0000000	0.0000000	0.0000000
0.0000000	0.0000000	0.0000000	0.0000000	0.0000000	0.0000000	0.0000000	0.0000000
0.0000000	0.0000000	0.0000000	0.0000000	0.0000000	0.0000000	0.0000000	0.0000000
0.0000000	0.0000000	0.0000000	0.0000000				

BLDAT	AANDK	ERSOR	STRFN	SLCRD	INTVL	SURVL
2	0	0	0	0	0	1

NACA 65(12)-10 CASCADE AT 0.71 INLET MACH NUMBER AND 16.5 DEGREE ANGLE OF ATTACK

GAM	AR	TIP	RHOIP	WTFL		OMEGA	ORF
1.400000	1716.480	519.9993	0.2371500E-02	0.2486520E-02	0.0000000	0.0000000	1.912930
BETAI	BETAO	CHORDF	STGRF	FSMI	FSMO		
45.08112	23.29999	0.2207009	0.1170300E-03	-0.1040900	0.3213000		
REDFAC	DENTOL	SSM1	SSM2				
0.9000000	0.9999999E-03	0.0000000	0.0000000				

MBI	MBO		MM	NBBI	NBL	NRSP
18	58	0 0	68	35	25145	28

BLADE SURFACE 1 -- UPPER SURFACE

RI1	RO1	BETI1	BETO1	SPLNO1
0.6549999E-02	0.3614998E-03	68.00000	5.000000	9.000000

MSP1 ARRAY

0.7499999E-03	0.6131999E-02	0.2175100E-01	0.4607900E-01	0.7673299E-01	0.1107100	0.1447000	0.1753500
0.2206800							

THSP1 ARRAY

0.2581600E-05	0.1251400E-04	0.3053500E-04	0.5131999E-04	0.7183600E-04	0.8897399E-04	0.1012400E-03	0.1098500E-03
0.1175300E-03							

BLADE SURFACE 2 -- LOWER SURFACE

RI2	RO2	BETI2	BETO2	SPLNO2
0.2075000E-02	0.3614998E-03	19.00000	10.00000	9.000000

MSP2 ARRAY

0.7499999E-03	0.6131999E-02	0.2175100E-01	0.4607900E-01	0.7673299E-01	0.1107100	0.1447000	0.1753500
0.2206800							

THSP2 ARRAY

-0.9219000E-06	-0.3295000E-06	0.9215600E-05	0.2418600E-04	0.4250499E-04	0.6262999E-04	0.8359399E-04	0.1009400E-03
0.1168500E-03							

MR ARRAY

-0.1507559	-0.1040879	-0.5742100E-01	-0.1075200E-01	0.3986999E-02	0.1872600E-01	0.3346500E-01	0.4820100E-01
0.6293797E-01	0.7767498E-01	0.9241396E-01	0.1071530	0.1218910	0.1366280	0.1513669	0.1661060
0.1808430	0.1955810	0.2103200	0.2250650	0.2398199	0.2545649	0.2693040	0.2953039
0.3213020	0.3473020	0.3733020	0.3993030				

RMSP ARRAY

1000.500	1000.500	1000.500	1000.500	1000.500	1000.500	1000.500	1000.500
1000.500	1000.500	1000.500	1000.500	1000.500	1000.500	1000.500	1000.500
1000.500	1000.500	1000.500	1000.500	1000.500	1000.500	1000.500	1000.500
1000.500	1000.500	1000.500	1000.500				

BESP ARRAY

0.9999998E-02	0.9999998E-02	0.9969998E-02	0.9939998E-02	0.9930000E-02	0.9919997E-02	0.9909999E-02	0.9904999E-02
0.9895999E-02	0.9886999E-02	0.9877998E-02	0.9868998E-02	0.9859998E-02	0.9849999E-02	0.9839997E-02	0.9829998E-02
0.9819999E-02	0.9809997E-02	0.9804998E-02	0.9799998E-02	0.9790000E-02	0.9779997E-02	0.9764999E-02	0.9749997E-02
0.9735998E-02	0.9735998E-02	0.9735998E-02	0.9735998E-02				

WOWCR ARRAY

0.7415709	0.7394069	0.7740059	0.7840120	0.7720060	0.7493449	0.7136109	0.6998169
0.6905439	0.6752990	0.6642340	0.6506020	0.6348169	0.6184919	0.6006330	0.5827349
0.5587429	0.5368910	0.5175950	0.5019590	0.5023980	0.5003590	0.5021140	0.5022910
0.5015700	0.5020820	0.5018750	0.5027380				

PLOSS ARRAY

0.0000000	0.0000000	0.0000000	0.0000000	0.0000000	0.0000000	0.0000000	0.0000000
0.0000000	0.0000000	0.0000000	0.0000000	0.0000000	0.0000000	0.0000000	0.0000000
0.0000000	0.0000000	0.0000000	0.0000000	0.0000000	0.0000000	0.0000000	0.0000000
0.0000000	0.0000000	0.0000000	0.0000000				

BLDAT	AANDK	ERSOR	STRFN	SLCRD	INTVL	SURVL
2	0	0	0	0	0	1

HIGH SOLIDITY AXIAL TURBINE STATOR AT 0.231 INLET CRITICAL VELOCITY RATIO

GAM	AR	TIP	RHOIP	WTFL		OMEGA	ORF
1.400000	287.0498	288.1499	1.224999	0.3619600	0.0000000	0.0000000	0.0000000
BETAI	BETAO	CHORDF	STGRF	FSMI	FSMO		
0.0000000	-67.00000	0.4290000E-01	-0.1108400	0.0000000	0.0000000		
REDFAC	DENTOL	SSM1	SSM2				
0.8000000	0.9999999E-03	0.0000000	0.0000000				

MBI	MBO			MM	NBBI	NBL	NRSP
15	49	0	0	63	33	50	13

BLADE SURFACE 1 -- UPPER SURFACE

RI1	RO1	BETI1	BETO1	SPLNO1			
0.3810000E-02	0.8889998E-03	28.29999	-72.79999	8.000000			
MSP1 ARRAY							
0.0000000	0.8575000E-02	0.1715000E-01	0.2572500E-01	0.3430000E-01	0.3858800E-01	0.4100000E-01	0.0000000
THSP1 ARRAY							
0.0000000	0.1769000E-01	0.1538000E-01	-0.5309999E-02	-0.4654000E-01	-0.7399994E-01	-0.9312999E-01	0.0000000

BLADE SURFACE 2 -- LOWER SURFACE

RI2	RO2	BETI2	BETO2	SPLNO2			
0.3810000E-02	0.8889998E-03	-14.20000	-56.79999	6.000000			
MSP2 ARRAY							
0.0000000	0.8575000E-02	0.1715000E-01	0.2572500E-01	0.3430000E-01	0.0000000		
THSP2 ARRAY							
0.0000000	-0.1562000E-01	-0.2854000E-01	-0.3707000E-01	-0.8249998E-01	0.0000000		

MR ARRAY							
-0.1766500E-01	-0.7569999E-02	0.0000000	0.6299999E-02	0.1262000E-01	0.1893000E-01	0.2523000E-01	0.3154000E-01
0.3785000E-01	0.4290000E-01	0.5047000E-01	0.5678000E-01	0.6056500E-01			
RMSP ARRAY							
0.3302000	0.3302000	0.3302000	0.3302000	0.3302000	0.3302000	0.3302000	0.3302000
0.3302000	0.3302000	0.3302000	0.3302000	0.3302000			
BESP ARRAY							
0.1016000	0.1016000	0.1016000	0.1012700	0.1008000	0.1002000	0.9964997E-01	0.9909999E-01
0.9864998E-01	0.9840000E-01	0.9840000E-01	0.9840000E-01	0.9840000E-01			
WOWCR ARRAY							
0.2410000	0.2530000	0.2810000	0.3250000	0.3900000	0.4870000	0.6170000	0.7390000
0.7790000	0.8239999	0.7670000	0.7810000	0.7810000			

BLDAT	AANDK	ERSOR	STRFN	SLCRD	INTVL	SURVL
2	0	0	1	0	1	1

```
HIGH SOLIDITY AXIAL TURBINE STATOR AT 0.243 INLET CRITICAL VELOCITY RATIO
     GAM              AR              TIP             RHOIP            WTFL                                OMEGA           ORF
   1.400000        287.0498        288.1499         1.224999        0.3802000       0.0000000       0.0000000       1.890400
    BETAI            BETAO           CHORDF           STGRF            FSMI            FSMO
  0.0000000       -67.00000       0.4290000E-01   -0.1108400       0.0000000       0.0000000
   REDFAC           DENTOL           SSM1            SSM2
  0.8000000       0.9999999E-03   0.0000000       0.0000000
  MBI    MBO                  MM   NBBI    NBL   NRSP
    15     49      0       0     63     33     50     13

   BLADE SURFACE 1  --  UPPER SURFACE
     RI1             RO1             BETI1           BETO1           SPLNO1
  0.3810000E-02   0.8889998E-03   28.29999        -72.79999        8.000000
     MSP1  ARRAY
  0.0000000       0.8575000E-02   0.1715000E-01   0.2572500E-01   0.3430000E-01   0.3858800E-01   0.4100000E-01   0.0000000
     THSP1  ARRAY
  0.0000000       0.1769000E-01   0.1538000E-01  -0.5309999E-02  -0.4654000E-01  -0.7399994E-01  -0.9312999E-01   0.0000000

   BLADE SURFACE 2  --  LOWER SURFACE
     RI2             RO2             BETI2           BETO2           SPLNO2
  0.3810000E-02   0.8889998E-03  -14.20000        -56.79999        6.000000
     MSP2  ARRAY
  0.0000000       0.8575000E-02   0.1715000E-01   0.2572500E-01   0.3430000E-01   0.0000000
     THSP2  ARRAY
  0.0000000      -0.1562000E-01  -0.2854000E-01  -0.5070000E-01  -0.8249998E-01   0.0000000

     MR  ARRAY
 -0.1765000E-01  -0.7569999E-02   0.0000000       0.6308999E-02   0.1262000E-01   0.1893000E-01   0.2524000E-01   0.3154000E-01
  0.3785000E-01   0.4290000E-01   0.5047000E-01   0.5678000E-01   0.6057000E-01
     RMSP  ARRAY
  0.3302000       0.3302000       0.3302000       0.3302000       0.3302000       0.3302000       0.3302000       0.3302000
  0.3302000       0.3302000       0.3302000       0.3302000       0.3302000
     BESP  ARRAY
  0.1016000       0.1016000       0.1016000       0.1012700       0.1007900       0.1002200       0.9963995E-01   0.9908998E-01
  0.9863997E-01   0.9840000E-01   0.9840000E-01   0.9840000E-01   0.9840000E-01
     WOWCR ARRAY
  0.2539999       0.2660000       0.2970000       0.3440000       0.4150000       0.5220000       0.6740000       0.8410000
  0.9000000       0.9669999       0.8850000       0.9200000       0.9150000

   BLDAT  AANDK  ERSOR  STRFN  SLCRD  INTVL  SURVL
     2      0      0      1      0      1      1
```

MULTIPLE CIRCULAR ARC COMPRESSOR STATOR AT 0.86 INLET CRITICAL VELOCITY RATIO

GAM	AR	TIP	RHOIP	WTFL		OMEGA	ORF
1.400000	1716.480	592.9778	0.3247100E-02	0.3249999E-03	0.0000000	0.0000000	0.0000000
LAMBDA	RVTHO	CHORDF	STGRF				
328.5999	24.16029	0.1130880	0.9560597E-01				
REDFAC	DENTOL	SSM1	SSM2				
0.8000000	0.9999999E-03	0.0000000	0.0000000				

MBI	MBO		MM	NBBI	NBL	NRSP
21	61	0 0	81	20	60	28

BLADE SURFACE 1 -- UPPER SURFACE

RI1	RO1	BETI1	BETO1	SPLNO1			
0.4475999E-03	0.4337998E-03	47.20630	-13.47120	13.00000			
MSP1 ARRAY							
0.1190000E-03	0.4005000E-02	0.1403600E-01	0.2422700E-01	0.3456800E-01	0.4503700E-01	0.5562300E-01	0.6631398E-01
0.7710600E-01	0.8799297E-01	0.9897095E-01	0.1100420	0.1127560			
THSP1 ARRAY							
0.6251000E-03	0.9152297E-02	0.2983930E-01	0.4888040E-01	0.6602407E-01	0.7977408E-01	0.8966607E-01	0.9661150E-01
0.1007981	0.1023905	0.1013961	0.9770727E-01	0.9645098E-01			

BLADE SURFACE 2 -- LOWER SURFACE

RI2	RO2	BETI2	BETO2	SPLNO2			
0.4475999E-03	0.4337998E-03	42.51540	-4.677400	13.00000			
MSP2 ARRAY							
0.7499999E-03	0.4005000E-02	0.1403600E-01	0.2422700E-01	0.3456800E-01	0.4503700E-01	0.5562300E-01	0.6631398E-01
0.7710600E-01	0.8799297E-01	0.9897095E-01	0.1100420	0.1126200			
THSP2 ARRAY							
-0.6781998E-03	0.5400296E-02	0.2314780E-01	0.3959020E-01	0.5473610E-01	0.6771237E-01	0.7782537E-01	0.8552259E-01
0.9100968E-01	0.9440929E-01	0.9578615E-01	0.9513259E-01	0.9473985E-01			
MR ARRAY							
-0.1500780	-0.1178589	-0.8627397E-01	-0.5522600E-01	-0.4534800E-01	-0.3547900E-01	-0.2561800E-01	-0.1575700E-01
-0.5890999E-02	0.4005000E-02	0.1403600E-01	0.2422700E-01	0.3456800E-01	0.4503700E-01	0.5562300E-01	0.6631398E-01
0.7710695E-01	0.8799297E-01	0.9897095E-01	0.1100420	0.1211210	0.1320640	0.1428739	0.1635180
0.1837190	0.2037770	0.2238040	0.2438010				
RMSP ARRAY							
0.4799400	0.4802030	0.4809170	0.4822360	0.4828160	0.4834720	0.4842030	0.4850060
0.4858740	0.4867989	0.4878560	0.4889980	0.4901280	0.4913880	0.4927790	0.4941829
0.4955370	0.4967880	0.4979129	0.4989139	0.4997590	0.5003800	0.5008200	0.5012569
0.5013770	0.5013320	0.5011660	0.5009050				
BESP ARRAY							
0.4342899E-02	0.4349299E-02	0.4351299E-02	0.4328497E-02	0.4312798E-02	0.4292600E-02	0.4267797E-02	0.4239399E-02
0.4209999E-02	0.4189599E-02	0.4169997E-02	0.4138298E-02	0.4093699E-02	0.4007597E-02	0.3932100E-02	0.3872600E-02
0.3825600E-02	0.3789900E-02	0.3765800E-02	0.3751900E-02	0.3745200E-02	0.3742000E-02	0.3744200E-02	0.3759600E-02
0.3779000E-02	0.3794600E-02	0.3804500E-02	0.3808000E-02				
WOWCR ARRAY							
0.8570000	0.8570000	0.8570000	0.8570000	0.8570000	0.8570000	0.8609999	0.8670000
0.8810000	0.8780000	0.8690000	0.8600000	0.8150000	0.7620000	0.7200000	0.6880000
0.6600000	0.6330000	0.6180000	0.6020000	0.5870000	0.5730000	0.5730000	0.5730000
0.5730000	0.5730000	0.5730000	0.5730000				
PLOSS ARRAY							
0.0000000	0.0000000	0.0000000	0.0000000	0.0000000	0.0000000	0.0000000	0.0000000
0.0000000	0.2420000E-02	0.8459996E-02	0.1463000E-01	0.2063000E-01	0.2639000E-01	0.3216000E-01	0.3789000E-01
0.4362000E-01	0.4935000E-01	0.5515000E-01	0.6113000E-01	0.6285000E-01	0.6298000E-01	0.6320000E-01	0.6372994E-01
0.6427997E-01	0.6465000E-01	0.6483996E-01	0.6483996E-01				

BLDAT	AANDK	ERSOR	STRFN	SLCRD	INTVL	SURVL
2	0	0	0	1	1	1

```
LOW SOLIDITY AXIAL TURBINE STATOR AT 0.334 INLET CRITICAL VELOCITY RATIO
     GAM              AR              TIP             RHOIP            WTFL                                OMEGA           ORF
   1.311000         1716.480        2385.000       0.2027800E-02   0.2429000E-02   0.0000000       0.0000000       0.0000000
    BETAI            BETAO          CHORDF            STGRF            FSMI            FSMO
   45.59999         66.50000       0.4166700E-01     0.3880820       0.0000000       0.0000000
    REDFAC           DENTOL           SSM1              SSM2
  0.8000000        0.4999999E-02   0.0000000         0.0000000
 MBI     MBO                    MM    NBBI     NBL    NRSP
   16      36      0       0     51      36      15      14

  BLADE SURFACE 1  --  UPPER SURFACE
     RI1              RO1             BETI1             BETO1           SPLNO1
 0.2083300E-02   0.6249999E-03    46.59999          62.50000          2.000000
    MSP1  ARRAY
 0.0000000        0.0000000
    THSP1  ARRAY
 0.0000000        0.0000000

  BLADE SURFACE 2  --  LOWER SURFACE
     RI2              RO2             BETI2             BETO2           SPLNO2
 0.2083300E-02   0.6249999E-03    40.59999          68.50000          3.000000
    MSP2  ARRAY
 0.0000000        0.1354200E-01   0.0000000
    THSP2  ARRAY
 0.0000000        0.4726000E-01   0.0000000

    MR  ARRAY
-0.3125000E-01  -0.1666700E-01  -0.2083300E-02   0.2083300E-02   0.4166700E-02   0.6249998E-02   0.8332998E-02   0.1041700E-01
 0.1250000E-01   0.2500000E-01   0.3958400E-01   0.4583000E-01   0.5833000E-01   0.7290000E-01
    RMSP  ARRAY
 0.1824999        0.1824999       0.1824999       0.1824999       0.1824999       0.1824999       0.1824999       0.1824999
 0.1824999        0.1824999       0.1824999       0.1824999       0.1824999       0.1824999
    BESP  ARRAY
 0.3265000E-01   0.3265000E-01   0.3265000E-01   0.3264200E-01   0.3261800E-01   0.3257600E-01   0.3251600E-01   0.3243500E-01
 0.3233300E-01   0.3120400E-01   0.2979500E-01   0.2976100E-01   0.2976200E-01   0.2976000E-01
    WOWCR ARRAY
 0.3340000        0.3340000       0.3370000       0.3900000       0.4060000       0.4250000       0.4480000       0.4780000
 0.5100000        0.7510000       0.8910000       0.8540000       0.8550000       0.8540000

  BLDAT  AANDK  ERSOR  STRFN  SLCRD  INTVL  SURVL
    2      0      0      0      1      1      1
```

CENTRIFUGAL COMPRESSOR SHROUD AT 1.168 INLET RELATIVE CRITICAL VELOCITY RATIO

GAM	AR	TIP	RHOIP	WTFL		OMEGA	ORF
1.400000	287.0398	288.1499	1.225060	0.2387360E-02	0.0000000	7853.938	1.837962
BETAI	BETAO	CHORDF	STGRF	FSMI	FSMO		
-61.00999	-45.00000	0.6320089E-01	-0.8931800	0.0000000	0.0000000		
REDFAC	DENTOL	SSM1	SSM2				
0.8000000	0.4999999E-02	-0.1040000	0.5500000E-02				

MBI	MBO		MM	NBBI	NBL	NRSP
10	55	0 0	65	20	19	16

BLADE SURFACE 1 -- UPPER SURFACE

RI1	RO1	BETI1	BETO1	SPLNO1			
0.1270000E-03	0.2549998E-03	-58.82999	-30.09999	12.00000			
MSP1 ARRAY							
0.0000000	0.3085000E-02	0.5999997E-02	0.1015094E-01	0.1395492E-01	0.1880579E-01	0.2580497E-01	0.3781136E-01
0.4700920E-01	0.5581425E-01	0.5969230E-01	0.6320089E-01				
THSP1 ARRAY							
0.0000000	-0.1030093	-0.2056858	-0.3360417	-0.4367357	-0.5378019	-0.6389605	-0.7401729
-0.7907768	-0.8411410	-0.8662432	-0.8931839				

BLADE SURFACE 2 -- LOWER SURFACE

RI2	RO2	BETI2	BETO2	SPLNO2			
0.1270000E-03	0.2549998E-03	-61.00999	-30.09999	12.00000			
MSP2 ARRAY							
0.0000000	0.3085000E-02	0.5999997E-02	0.1015094E-01	0.1395492E-01	0.1880579E-01	0.2580497E-01	0.3781136E-01
0.4700920E-01	0.5581425E-01	0.5969230E-01	0.6320089E-01				
THSP2 ARRAY							
0.0000000	-0.1211222	-0.2244458	-0.3540897	-0.4533958	-0.5523296	-0.6511711	-0.7499586
-0.7993546	-0.8489904	-0.8738883	-0.8931839				

MR ARRAY							
-0.1400000E-01	-0.6999999E-02	0.0000000	0.3085000E-02	0.5999997E-02	0.1015094E-01	0.1395492E-01	0.1880580E-01
0.2580497E-01	0.3781136E-01	0.4700920E-01	0.5581425E-01	0.5969230E-01	0.6320089E-01	0.7020086E-01	0.7720089E-01
RMSP ARRAY							
0.4445000E-01	0.4445000E-01	0.4445000E-01	0.4445000E-01	0.4445000E-01	0.4453529E-01	0.4485670E-01	0.4572480E-01
0.4805373E-01	0.5517900E-01	0.6279075E-01	0.7112956E-01	0.7496494E-01	0.7846957E-01	0.8546954E-01	0.9249997E-01
BESP ARRAY							
0.8326999E-03	0.8326999E-03	0.8101000E-03	0.7757000E-03	0.7257999E-03	0.6490999E-03	0.5756000E-03	0.4906999E-03
0.3991998E-03	0.2803998E-03	0.2043000E-03	0.1571000E-03	0.1465000E-03	0.1449000E-03	0.1492000E-03	0.1492000E-03
WOWCR ARRAY							
1.158000	1.158000	1.094999	0.9600000	0.9750000	0.9680000	0.9349999	0.8950000
0.8600000	0.7950000	0.7600000	0.6700000	0.6199999	0.6170000	0.7150000	0.8500000

BLDAT	AANDK	ERSOR	STRFN	SLCRD	INTVL	SURVL
2	0	0	0	1	1	1

References

1. Katsanis, Theodore: Fortran Program for Calculating Transonic Velocities on a Blade-to-Blade Stream Surface of a Turbomachine. NASA TN D-5427, 1969.
2. Katsanis, Theodore and McNally, William D: Fortran Program for Calculating Velocities and Streamlines on a Blade-to-Blade Stream Surface of a Tandem Blade Turbomachine. NASA TN D-5044, 1969.
3. Katsanis, Theodore; and McNally, William D: Fortran Program for Calculating Velocities in a Magnified Region on a Blade-to-Blade Stream Surface of a Turbomachine. NASA TN D-5091. 1969.
4. Shapiro, Ascher H.: The Dynamics and Thermodynamics of Compressible Flow. Vol. I. Ronald Press Co., 1953.
5. Katsanis, Theodore, and McNally, William D.: Revised FORTRAN Program for Calculating Velocities and Streamlines on the Hub-Shroud Mid-Channel Stream Surface of an Axial-, Radial-, or Mixed-Flow Turbomachine or Annular Duct. I—User's Manual. NASA TN D-8430, 1977.
6. Vanco, Michael R.: Fortran Program for Calculating Velocities in the Meridional Plane of a Turbomachine I—Centrifugal Compressor. NASA TN D-6701, 1972.
7. Wu, Chung-Hua: A General Theory of Three-Dimensional Flow in Subsonic and Supersonic Turbomachines of Axial-, Radial-, and Mixed-Flow Types, NACA TN 2604, 1952.
8. Briggs, William B.: Effect of Mach Number on the Flow and Application of Compressibility Corrections in a Two-Dimensional Subsonic-Transonic Compressor Cascade Having Varied Porous-Wall Suction at the Blade Tips. NACA TN 2649, 1952.
9. Herrig, L. Joseph; Emery, James C.; and Erwin, John R.: Systematic Two-Dimensional Cascade Tests of NACA 65 Series Compressor Blades at Low Speeds. NACA RM L51G31, 1951.
10. Whitney, Warren J.; Szanca, Edward M.; Moffitt, Thomas P.; and Monroe, Daniel E.: Cold-Air Investigation of a Turbine for High-Temperature Engine Application. NASA TN D-3751, 1967.
11. Stephens, H.E.: Application of Supercritical Airfoil Technology to Compressor Cascades: Comparison of Theoretical and Experimental Results. AIAA Paper 78-1138, July 1978.

1. Report No. NASA TP-1772	2. Government Accession No.	3. Recipient's Catalog No.
4. Title and Subtitle IMPROVED METHOD FOR CALCULATING TRANSONIC VELOCITIES ON BLADE-TO-BLADE STREAM SURFACES OF A TURBOMACHINE		5. Report Date April 1981 6. Performing Organization Code 505-32-2A
7. Author(s) Jerry R. Wood		8. Performing Organization Report No. E-128 10. Work Unit No.
9. Performing Organization Name and Address National Aeronautics and Space Administration Lewis Research Center Cleveland, Ohio 44135		11. Contract or Grant No.
12. Sponsoring Agency Name and Address National Aeronautics and Space Administration Washington, D.C. 20546		13. Type of Report and Period Covered Technical Paper 14. Sponsoring Agency Code

15. Supplementary Notes

16. Abstract

A method has been developed to improve the accuracy of an existing computer program that is used to calculate transonic velocities on a blade-to-blade surface of a turbomachine. The method eliminates problems previously encountered in obtaining adequate solutions with the velocity gradient equation when large gradients in velocity occur through the blade row. With the improved method, results also indicate that the transonic solution can be obtained by scaling the velocities obtained at the reduced mass flow rate where all velocities are subsonic thereby eliminating the need for a solution of the velocity gradient equation. Solutions obtained with the scaling method on a two-dimensional compressor cascade and an axial turbine stator show good agreement with experimental data. The results obtained for the stationary blade rows and comparison of analytical results obtained with and without the present method suggest that the method will yield an improved solution for centrifugal compressor impellers.

17. Key Words (Suggested by Author(s))	18. Distribution Statement
Transonic; Turbomachine flow; Blade-to-blade	Unclassified - unlimited STAR Category 02

19. Security Classif. (of this report)	20. Security Classif. (of this page)	21. No. of Pages	22. Price*
Unclassified	Unclassified	27	A03

* For sale by the National Technical Information Service, Springfield, Virginia 22161

NASA-Langley, 1981

9 1 1U,A, 041081 S00903DS
DEPT OF THE AIR FORCE
AF WEAPONS LABORATORY
ATTN: TECHNICAL LIBRARY (SUL)
KIRTLAND AFB NM 87117